IMPACT OF URBANIZATION ON URBAN HEAT ISLAND INTENSITY IN MYMENSINGH, BANGLADESH: A STUDY USING LANDSAT-8 IMAGES ON GOOGLE EARTH ENGINE

Md. Istiak Hossain*[1] and Jahidul Islam[2]

[1] *Undergraduate Student, Rajshahi University of Engineering & Technology, Bangladesh, e-mail:*
istiakhossainsazid2019@gmail.com
[2] *Undergraduate Student, Rajshahi University of Engineering & Technology, Bangladesh, e-mail:*
jahidulislam261431@gmail.com

*Corresponding Author

ABSTRACT

Growth in urban areas greatly impacts land surface temperature (LST), which is influenced by alterations in land use/land cover (LULC) patterns. This contributes to the degree of urban heat islands (UHI). Resource shortages along with growing urbanization in areas with high populations lead to the direct and indirect effects of rising temperature levels in cities on the local population. UHI analyses are crucial in rising cities to evaluate the potential harm they might trigger, such as higher energy occupancy, worsening air quality, and an upsurge in the rate of heat-related sickness in urban surroundings. To date, nothing particular is known about the precise character of UHI changes in Mymensingh, a part of Bangladesh that is continuously urbanizing. The spatiotemporal trends in UHI intensity in the years 2014, 2018, and 2022 were investigated in this work employing cutting-edge remote sensing tools. The investigation we conducted revolves around Mymensingh, a region witnessing notable urban evolution, and makes use of the features of the Google Earth Engine (GEE) platform with Landsat-8 imagery. The urbanization rate in Mymensingh increased from 8.33% in 2014 to 22.93% in 2022. This upward trend was matched by a corresponding rise in the proportion of bare land, which grew from 7.27% to 20.23%, where there was a drop in vegetation and water bodies, with percentages declining from 72.21% and 12.19% to 50.30% and 6.54%, respectively at the identical time span. The observed phenomenon was correlated with an upsurge in LST ranging from 18.65–32.02°C to 21.43–39.75°C, as well as an escalation in UHI intensity from a range of -6.21 to 7.72°C to a range of -8.82 to 11.76°C at the identical time span. Taking into consideration the outcomes, appropriate solutions may be implemented to cope with expanding suburbanization, which serves as a crucial step to lessen the intensity of the UHI. The detected variation in UHI intensity throughout the investigated area raises questions about how it can affect local climate behavior. Most importantly, the findings of our study provide policymakers with information that they can use to put into effect strategies to mitigate the effects of UHI and address climate-related problems in Mymensingh, protecting the overall health of people living there and potentially serving as a blueprint for territories dealing with comparable urbanization difficulties.

Keywords: *LULC; LST; UHI; GEE; climate; Mymensingh*

1. INTRODUCTION

Urbanization, exemplified by the development of highways, industries, and structures has an enormous effect on climatic conditions by triggering a rise in atmospheric temperature and the release of carbon emissions, resulting in the formation of an urban heat island (UHI) (Muñoz et al., 2020). The phenomenon includes the movement of populations, socioeconomic transformations, alterations in physical geography, and other distinctions in land surface examination (Seto et al., 2014).

Human activities, including land use and land cover (LULC) changes, have a significant impact on the earth's radiation balance, resulting in a rise in temperature at the surface. The phenomenon is referred to as the UHI (Connors et al., 2013). The UHI effect refers to the phenomenon whereby metropolitan regions exhibit greater temperatures compared to suburban along with countryside areas. The elevated land surface temperature (LST) seen in urban areas may be attributed to the UHI effect, which exhibits a progressive decline in vegetated countryside (McCarthy et al., 2010).

Structurally compacted suburbs exhibit a phenomenon of evolving temperature rise, resulting in the amplification of the UHI effect in urban centers as opposed to the countryside (Chapman et al., 2019). Multiple prior studies have shown that the extensive spread of heat is influenced by factors such as building design, land use patterns, and industrial development. This phenomenon leads to an elevation in LST inside cities as well as suburbs (Abir et al., 2021; Morshed et al., 2021). The development of urban structures, population growth, and other human-made structures contribute to the expansion of the UHI effect. This phenomenon has a significant influence on the regional climate, leading to a reduction in precipitation, evapotranspiration, and the standard of air and water. These changes have adverse effects on human wellness and living circumstances, as supported by previous studies (Ayanlade, 2017). The UHI effect may have detrimental health effects by altering rainfall patterns, aggravating air pollution, raising the risk of flooding, and lowering water quality (Heaviside et al., 2017). People are directly impacted by UHI because it exposes them to high temperatures, particularly during extreme temperatures, and globally, a large body of evidence connects exposure to hot or cold temperatures to higher rates of disease, hospitalization, and death (Gasparrini et al., 2015). Thus, UHIs have lately been a focus of attention amongst numerous research experts.

Various methodologies have been used to elucidate urban climate phenomena and the alteration of LST, which may be effectively proven using both ground-based and satellite measurements. The field of planet observation, which involves the evaluation of the Earth's surface from the ground, relies on station-based assessments to examine the difference in air temperature caused by the UHI effect (Kim & Brown, 2021). However, prior studies have shown significant impacts on satellite-based observation systems when it comes to retrieving LST and measuring UHI in terms of space and time (Maharjan et al., 2021). The adoption of LULC is used as a means to detect UHI (Rani et al., 2018). Furthermore, the identification of LULC patterns is facilitated by fast urbanization and significant residential expansion. However, the analysis of urban areas, particularly the examination of seasonal fluctuations in vegetation and the assessment of LULC categories ranging from undeveloped to developed, has proven to be intricate. Several satellite-based indices, such as the soil-adjusted vegetation index, the normalized difference building index, and the normalized difference drought index, have been shown to be inadequate for observing built-up and barren terrain (Yang et al., 2017). This issue arises because of the challenges associated with pixel couplings in relation to the spectral response of diverse LULC categories, including water bodies, vegetation, barren ground, and built-up areas (Souza Jr et al., 2020). In this study, a coupling index including LULC, LST, and UHI utilizing Google Earth Engine (GEE) was used to address this challenge. The GEE platform is a robust tool for using big data due to its ability to do satellite imagery analysis via cloud-based processing, eliminating the need for local storage of information. The GEE is a robust tool for using enormous amounts of data due to its ability to execute satellite imagery assessment via cloud-based interpreting, eliminating the need for physical storage of information.

Although an abundance of investigation has been done in Bangladesh regarding the influence of shifts in LULC on LST and UHI in urban areas, there is a lack of studies examining the intensity of UHI trend

in developing urban areas, most notably Mymensingh. To assess the complex effects of urbanization on the severity of UHI in swiftly urbanizing Mymensingh district, this study pioneers the combination of high-resolution Landsat-8 imagery with innovative analytic tools on the GEE platform. In contrast to other investigations that either had a wider region or utilized a restricted data sampling approach, the present study narrows its focus exclusively on Mymensingh, therefore offering an in-depth analysis of the unique UHI's temporal and geographical dynamics within this area. The key goals of this study are to (i) investigate the spatiotemporal relationships between UHI intensity in the years 2014, 2018, and 2022; and (ii) assess the impact of urban LULC shifts on the variability of UHI and LST trends in Mymensingh. The findings of this study have significance in the development of location-specific adaptation measures aimed at mitigating the environmental impacts resulting from urbanization-induced LST rising. Additionally, these findings have the potential to improve the overall well-being of urban dwellers.

2. STUDY AREA

The Mymensingh district stands in the central-northern portion of Bangladesh. The location coordinates of Mymensingh were identified to be 24.743448° N latitude and 90.4073° E longitude. The primary feature of the geographical locations in this area is the presence of flat land, sometimes interspersed with modest mountains. The geographical extent of the district is roughly 4,363 km^2, including a wide variety of land uses and ecological environments. The Brahmaputra River, an important topographical characteristic, flows through the area, exerting an influence on the local weather conditions. Mymensingh district is comprised of a total of thirteen upazilas. The local economy of the area is mostly reliant on the agricultural sector, where crops like rice, jute, and vegetables assume a crucial role. Mymensingh is situated in close proximity to the Garo Hills of Meghalaya in India, to the north. To the south lies Gazipur, while Netrokona and Kishoreganj mark the eastern periphery. The western boundary is marked by ancient forests such as Muktagacha and Valuka Upazilas, as well as the Chars of Jamalpur District to the northwest of Mymensingh. The illustration in Figure 1 depicts the location map of Mymensingh.
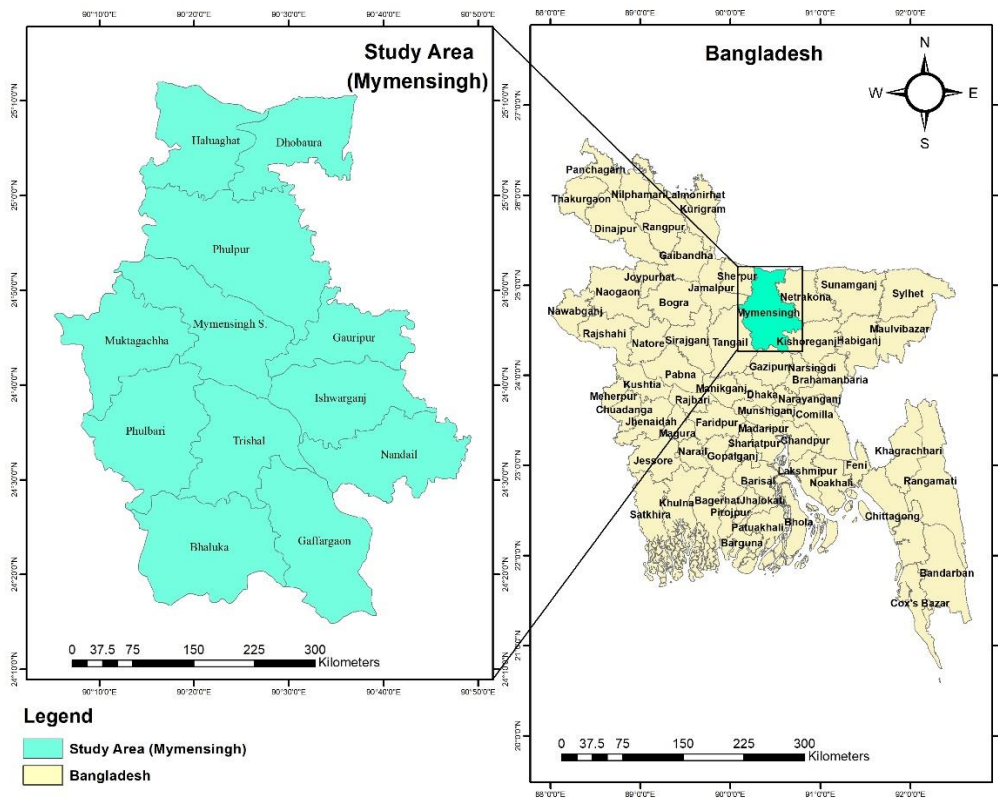

Figure 1: Location map of Mymensingh

3. METHODOLOGY

The investigation employed Landsat 8 images inside the GEE to conduct a thorough evaluation of LULC, LST, and UHI. A careful selection was made of images captured in the years 2014, 2018, and 2022, ensuring that they had minimum cloud cover. The detection of LULC classes was accomplished by the use of supervised classification. Furthermore, the LST was estimated by employing radiative transfer equations and thermal bands. The determination of UHI included a comparison between the values of LST in urban and rural regions. The generation of output raster data was conducted using GEE, followed by its importation into ArcGIS 10.8 for the purpose of building the final maps. Figure 2 depicts the flow chart illustrating the approaches utilized in the estimation of LULC, LST, and UHI.
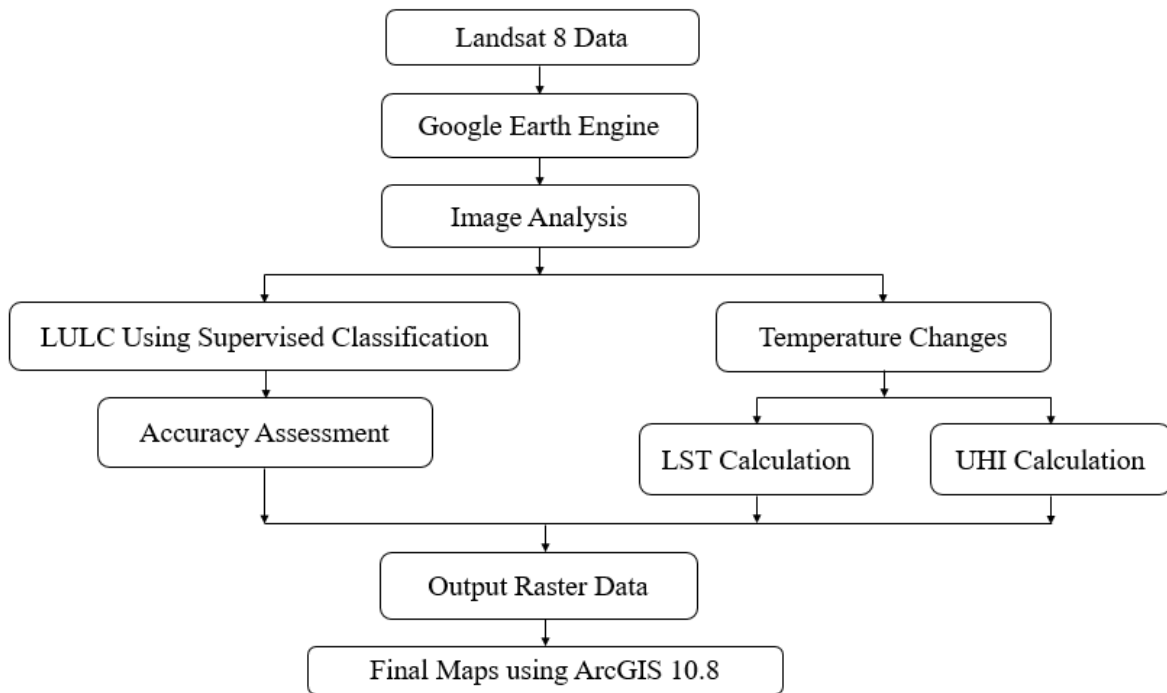
Figure 2: Flow chart conveying methodology

3.1 LULC Classification

The categorization of LULC was performed using imagery obtained from Landsat-8. The LULC classification was conducted using the maximum likelihood supervised classification (MLSC) method, with training sample regions used for this purpose. The photographs were classified into four categories: bare land, built-up area, vegetation, and water body. In order to build LULC maps, a total of around 50 to 60 samples were obtained for every individual class.

3.2 Accuracy Assessment

Roughly 200-250 ground monitoring points were employed to demonstrate the validation of the LULC map within the specified area for the years 2014, 2018, and 2022. The validity of the points was confirmed using Google Earth Pro. The researchers conducted the kappa coefficient assessment in order to quantitatively assess the degree of agreement.

3.3 LST Estimation

Numerous techniques, including split-window (SW), dual-angle (DA), and single-channel (SC), can be used to estimate LST (Solanky et al., 2018). In this paper, the SW algorithm is used to extract the LST. Following are the comprehensive steps for LST extraction pursued by numerous scholars (Avdan and Jovanovska, 2016; Gohain et al., 2021; Kafy et al., 2020).

3.3.1 Calculation of Top of Atmosphere (TOA) Spectral Radiance

Once Band 10 was input, the following formula was used to get the TOA spectral radiance (L_λ), which was obtained from the USGS:

$$L_\lambda = ML \times Qcal + AL - 0.29 \tag{1}$$

Where Qcal indicates the Landsat imagery's Band 10, ML is the band's multiplicative rescaling variable, and AL is the metadata file's additive rescaling factor associated with satellite visuals.

3.3.2 TOA to Brightness Temperature (BT) Transformation

The subsequent formula was executed to transform TOA to BT:

$$BT = \frac{k_2}{\ln(\frac{k_1}{L_\lambda}+1)} - 273.15 \tag{2}$$

The band-specific thermal conversion constants, K_1 and K_2, are derived from the metadata. The symbol L_λ represents the TOA spectral brightness. The radiant temperature may be converted to Celsius by subtracting the value of absolute zero, which is about -273.15 °C.

3.3.3 NDVI

The formula outlined later is employed to compute NDVI:

$$NDVI = (NIR-RED) / (NIR+RED) \tag{3}$$

3.3.4 Proportion of Vegetation(PV)

The measurement of vegetation proportion (PV) was carried out by using the greatest and least values of NDVI.

$$PV = [(NDVI - NDVI_{min}) / (NDVI_{max} + NDVI_{min})]^2 \tag{4}$$

3.3.5 Land Surface Emissivity (LSE)

The equation noted is the one employed for the estimation of LSE.

$$LSE = 0.004 \, PV + 0.986 \tag{5}$$

3.3.6 Land Surface Temperature (LST)

The equation mentioned is employed for the computation of LST, expressed in °C.

$$T = BT / [\, 1 + (\, \gamma \frac{BT}{\rho}\,) \ln (LSE)] \tag{6}$$

The symbol, γ is the wavelength of emanated radiance, while ρ is h x c/ σ =1.4388×10^{-2} mK, where h denotes Plank's constant, which is 6.626×10^{-34} Js, σ represents Boltzmann constant, which is 1.38×10^{-23} J/K and c denotes the velocity of light which is 2.998×10^8 m/s.

3.4 UHI Estimation

The notion of UHI is frequently characterized as the disparity between countryside and urban regions. The concept can additionally be characterized by quantification, which considers the impact of urban surfaces on both local and national climate change (Hu et al., 2019). The UHI calculation incorporated the LST (Rahman et al., 2022).

$$UHI = (T-T_m) / T_{sd} \qquad\qquad\qquad (7)$$

Where T symbolizes LST, T_m indicates the mean LST, while T_{sd} represents the standard deviation of LST.

4. RESULTS AND DISCUSSION

4.1 LULC Changes

Figure 3 illustrates LULC alterations that occurred in the region of Mymensingh over 2014, 2018, and 2022. On the basis of 2014, urban areas comprised 8.33% of the overall land area, while bare land took up 7.27%, water bodies and vegetation took up 12.19%, and 72.21%, correspondingly. In 2018, there was a significant rise in urban areas, reaching 15.21%. Additionally, bare land was expanded, which increased to 12.57%. Conversely, water bodies had a modest reduction, reaching a rate of 9.91%. The vegetation cover, however, saw a drop, accounting for 62.31% of the total area. By the year 2022, there had been a notable growth in urban areas, resulting in the occupation of 22.93% of the area. This urban expansion was followed by a significant rise in the amount of bare land, which accounted for 20.23% of the overall area. The proportion of water bodies decreased to 6.54%, indicating probable environmental changes, while vegetation saw a notable decline, covering 50.30% of the area. The observed changes in LULC statistics from 2014 to 2022 indicate a substantial alteration in the physical characteristics of the environment. The observed rise in urbanization signifies a fast progression of urban growth, which may affect natural habitats and the environment. Concurrently, the decrease in vegetation coverage implies probable ecological difficulties and a reduction in green areas that support biodiversity.
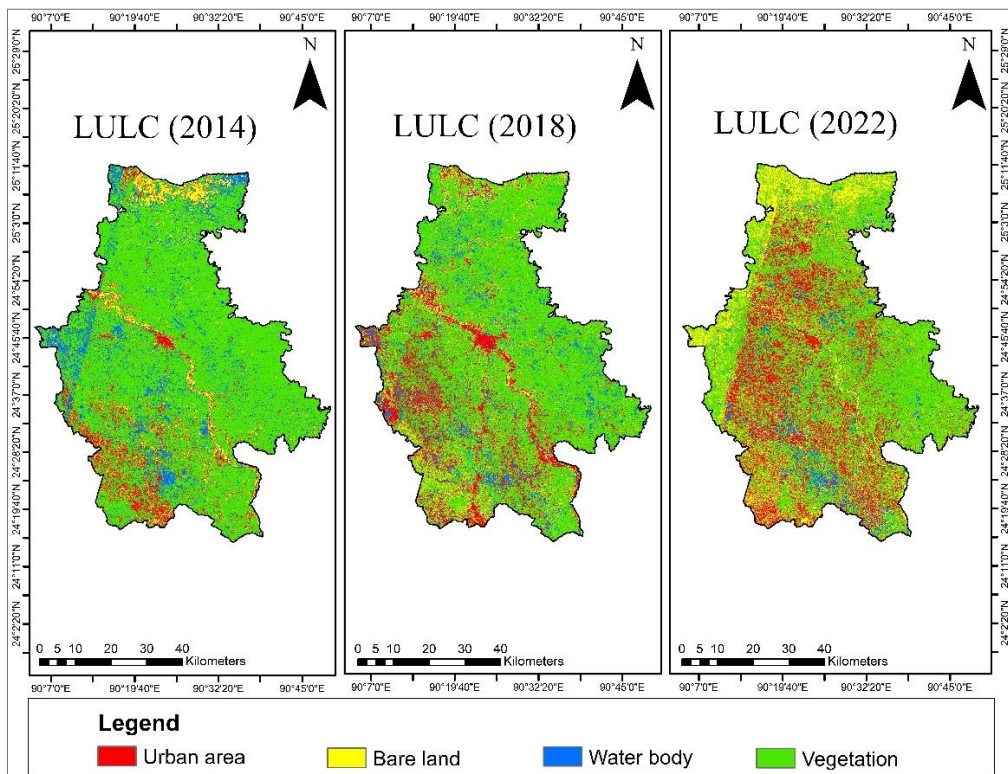

Figure 3: Spatiotemporal distributions of LULC in Mymensingh

4.2 Accuracy Assessment

The evaluation of accuracy has significant importance in the context of urban growth and the measurement of surface temperature. The current study adopted accuracy evaluation to verify the LULC categorization, which is illustrated in Table 4. The kappa coefficient and overall accuracy values demonstrate a level of over 80% for all LULC categorizations. The estimated value presented in the current analysis provides compelling evidence to support the classification of Mymensingh. A kappa value greater than 0.75 considerably denotes a high level of accuracy in classification (Rahman and Shozib, 2021).

Table 1: Accuracy assessment and kappa statistics

	User Accuracy (%)				Producer Accuracy (%)				Overall accuracy	Kappa statistics
Year	Vege-tation	Urban area	Bare land	Water body	Vege-tation	Urban area	Bare land	Water body		
2014	92.35	80.87	82.78	97.50	85.72	82.64	83.33	82.57	87.83	0.86
2018	94.56	82.58	85.65	95.48	91.67	81.29	83.33	89.19	89.33	0.88
2022	88.14	81.67	88.28	93.53	87.48	84.31	86.58	87.46	84.13	0.84

4.3 LST Assessment

Figure 4 reveals fluctuations in LST in Mymensingh between the years 2014 and 2022. The LST in 2014 had very small variability, with values ranging from 18.65 to 32.02°C. The aforementioned finding implies the presence of a thermally equitable environment throughout the region. Nevertheless, a noticeable change took place in 2018, as the range of LST expanded to 19.93–35.01°C. The apparent rise in temperature in the area is evident. The year 2022 had a notable and remarkable change, as the LST experienced a significant increase, reaching a range of 21.43–39.75°C.

The significant increase in temperature has wide-ranging consequences for the surrounding environment, ecology, and human welfare. An upsurge in LST may be ascribed to the simultaneous shifts in LULC patterns. The observed rise in urbanization and the prevalence of bare land are indicative of the growth of man-made surfaces and a drop in vegetation. The aforementioned alterations give rise to the phenomenon known as the UHI effect, whereby urbanized regions exhibit a propensity to soak up and store a greater amount of heat, thereby leading to elevated temperatures in comparison to the adjacent countryside. The exacerbation of this impact is intensified by the reduction in water bodies and vegetation since they provide vital functions for dropping temperature via the processes of evaporative cooling.
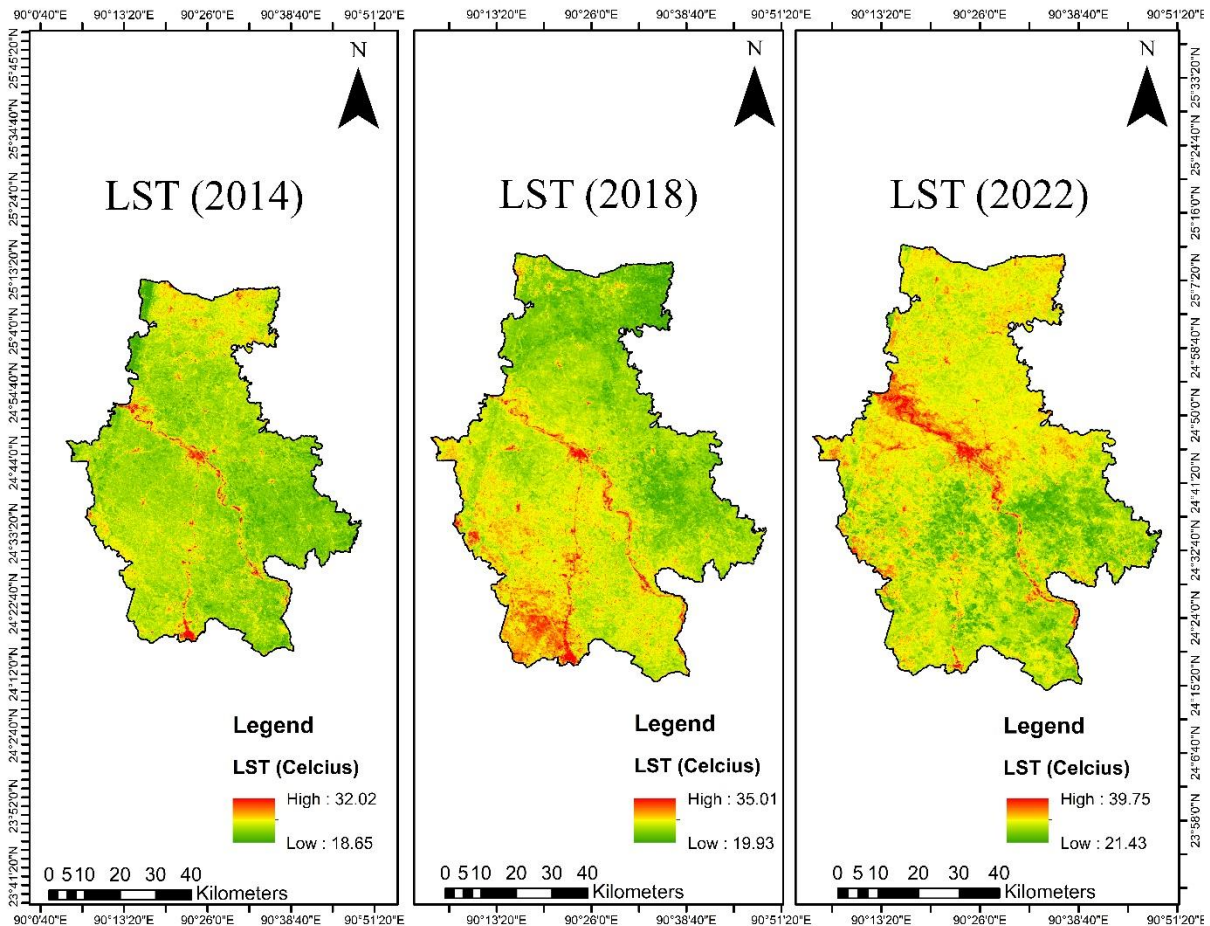
Figure 4: Spatiotemporal distributions of LST in Mymensingh during 2014-2022

4.4 UHI Intensity Assessment

Figure 5 depicts the UHI phenomenon for 2014, 2018, and 2022 in Mymensingh. The UHI detected in Mymensingh has shown an abrupt rise in intensity over time, as indicated by the observed variations in temperature. In the year 2014, the UHI exhibited a temperature range of -6.21 to 7.72°C, suggesting a considerable thermal dispersion between urban and non-urban parts. By the year 2018, the fluctuation of temperatures associated with the UHI effect had increased to an interval of -6.53 to 9.02°C. This expansion indicates a noticeable increase in the intensity of the UHI effect, which is in line with the noted rise in LST over the same time frame. The period of most significant escalation occurred between 2018 and 2022, during which the UHI range expanded from -8.82 to 11.76°C. This expansion signifies a major increase in thermal contrast. The observed significant rise in UHI intensity is consistent with the simultaneous changes in LULC patterns. The expansion of urban areas and the conversion of bare land, along with the decline of vegetation and water bodies, are symptomatic of the increasing urban footprint. These modifications have a substantial role in the reported increase in LST and therefore, the intensified UHI phenomenon. Urbanized and bare land have an inclination to soak up and store a greater amount of heat, contributing to increased temperatures. The UHI effect highlights the pressing demand for the enactment of tactical urban planning strategies that give precedence to ecological land use tactics.
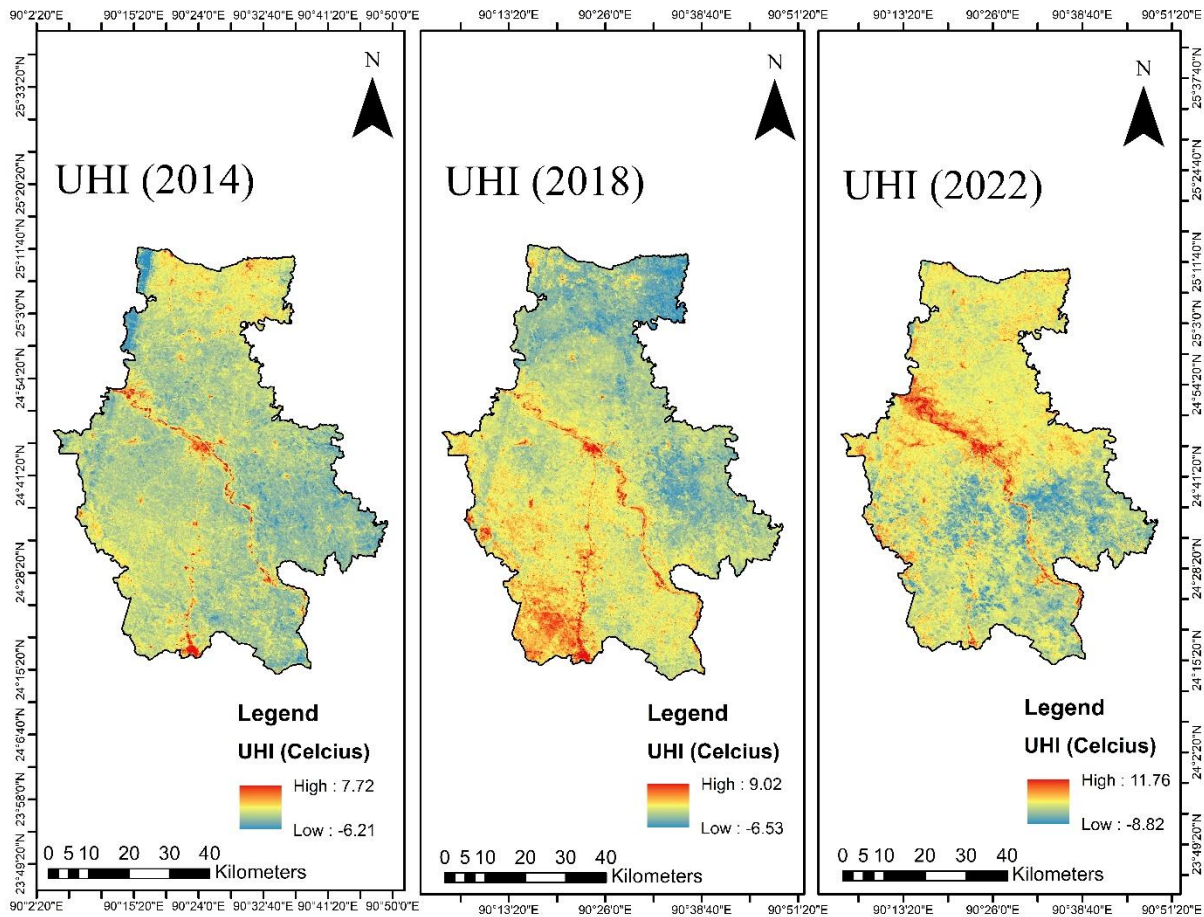
Figure 5: Spatiotemporal distributions of UHI intensity in Mymensingh during 2014-2022

5. CONCLUSION

Urbanization is a widespread and prevalent worldwide occurrence that has substantial environmental ramifications. The city of Mymensingh has seen significant urban expansion in the last few decades, resulting in notable alterations in LULC patterns. A comprehensive comprehension of the resultant implications for the intensity of UHI is important in order to facilitate efficient urban planning and the formulation of climate adaptation measures. The objective of this research was to examine the relationship among LULC changes, LST trends, and UHI intensity employing Landsat-8 images on GEE in Mymensingh throughout the period from 2014 to 2022. The outcomes of this investigation indicate that Mymensingh is undergoing a process of urbanization, leading to a spike in LST and an intensification of the UHI effect. From 2014 to 2022, there was an upsurge in the proportion of urban area and bare land, which grew from 8.33% to 22.93% and 7.27% to 20.23%, respectively, where there was a drop in vegetation and water bodies, with percentages declining from 72.21% and 12.19% to 50.30% and 6.54%, correspondingly at the identical time span. The phenomenon of urbanization persisted throughout the years, resulting in a concomitant rise in LST and UHI intensity. In 2014, the LST exhibited a range of 18.65–32.02°C, which increased to a range of 21.43–39.75°C in 2022. Similarly, the UHI intensity varied from -6.21 to 7.72°C in 2014, and this range expanded to -8.82 to 11.76°C in 2022.

The outcomes emphasize the urgent need for the implementation of sustainable urban planning strategies in the city of Mymensingh. The growing UHI phenomenon presents potential hazards to public health, energy use, and the general quality of urban environments. Moreover, the decrease in plant life and aquatic resources serves as an indication of ecological issues and emphasizes the need to conserve ecological systems within urban settings. In order to enhance the understanding of urban expansion and its influence on UHI intensity, further studies should use sophisticated modeling techniques for accurate forecasting. The incorporation of socio-economic and meteorological

information will provide a comprehensive perspective on the complex variables that shape urbanization and how it affects the environment in Mymensingh.

REFERENCES

Abir, F. A., Ahmmed, S., Sarker, S. H., & Fahim, A. U. (2021). Thermal and ecological assessment based on land surface temperature and quantifying multivariate controlling factors in Bogura, Bangladesh. *Heliyon*, *7*(9).

Avdan, U., & Jovanovska, G. (2016). Algorithm for automated mapping of land surface temperature using LANDSAT 8 satellite data. *Journal of sensors*, 2016, 1-8.

Ayanlade, A. (2017). Remote sensing approaches for land use and land surface temperature assessment: A review of methods. *International Journal of Image and Data Fusion*, *8*(3), 188-210.

Chapman, S., Thatcher, M., Salazar, A., Watson, J. E., & McAlpine, C. A. (2019). The impact of climate change and urban growth on urban climate and heat stress in a subtropical city. *International Journal of Climatology*, *39*(6), 3013-3030.

Connors, J. P., Galletti, C. S., & Chow, W. T. (2013). Landscape configuration and urban heat island effects: assessing the relationship between landscape characteristics and land surface temperature in Phoenix, Arizona. *Landscape ecology*, 28, 271-283.

Gasparrini, A., Guo, Y., Hashizume, M., Lavigne, E., Zanobetti, A., Schwartz, J., ... & Armstrong, B. (2015). Mortality risk attributable to high and low ambient temperature: a multicountry observational study. The lancet, 386(9991), 369-375.

Gohain, K. J., Mohammad, P., & Goswami, A. (2021). Assessing the impact of land use land cover changes on land surface temperature over Pune city, India. *Quaternary International*, 575, 259–269.

Heaviside, C., Macintyre, H., & Vardoulakis, S. (2017). The urban heat island: implications for health in a changing environment. Current environmental health reports, 4, 296-305.

Hu, Y., Hou, M., Jia, G., Zhao, C., Zhen, X., & Xu, Y. (2019). Comparison of surface and canopy urban heat islands within megacities of eastern China. *ISPRS Journal of Photogrammetry and Remote Sensing*, 156, 160-168.

Kafy, A. A., Faisal, A. A., Sikdar, S., Hasan, M., Rahman, M., Khan, M. H., & Islam, R. (2020). Impact of LULC changes on LST in Rajshahi district of Bangladesh: a remote sensing approach. *Journal of Geographical Studies*, 3(1), 11-23.

Kim, S. W., & Brown, R. D. (2021). Urban heat island (UHI) intensity and magnitude estimations: A systematic literature review. *Science of The Total Environment*, *779*, 146389.

Maharjan, M., Aryal, A., Man Shakya, B., Talchabhadel, R., Thapa, B. R., & Kumar, S. (2021). Evaluation of Urban Heat Island (UHI) Using Satellite Images in Densely Populated Cities of South Asia. *Earth*, *2*(1), 86-110.

McCarthy, M. P., Best, M. J., & Betts, R. A. (2010). Climate change in cities due to global warming and urban effects. *Geophysical research letters*, 37(9).

Morshed, S. R., & Fattah, M. A. (2021). Responses of spatiotemporal vegetative land cover to meteorological changes in Bangladesh. *Remote Sensing Applications: Society and Environment*, *24*, 100658.

Muñoz, P., Zwick, S., & Mirzabaev, A. (2020). The impact of urbanization on Austria's carbon footprint. *Journal of Cleaner Production*, *263*, 121326.

Rahman, M. N., & Shozib, S. H. (2021). Seasonal variability of waterlogging in Rangpur city corporation using GIS and remote sensing techniques. *Geosfera Indonesia*, 6(2), 143-156.

Rahman, M. N., Rony, M. R. H., Jannat, F. A., Chandra Pal, S., Islam, M. S., Alam, E., & Islam, A. R. M. T. (2022). Impact of urbanization on urban heat island intensity in major districts of Bangladesh using remote sensing and geo-spatial tools. *Climate*, 10(1), 3.

Rani, M., Kumar, P., Pandey, P. C., Srivastava, P. K., Chaudhary, B. S., Tomar, V., & Mandal, V. P. (2018). Multi-temporal NDVI and surface temperature analysis for Urban Heat Island inbuilt surrounding of sub-humid region: A case study of two geographical regions. *Remote Sensing Applications: Society and Environment*, *10*, 163-172.

Seto, K. C., Dhakal, S., Bigio, A., Blanco, H., Carlo Delgado, G., Dewar, D., Huang, L., Inaba, A., Kansal, A., Lwasa, S. & Zwickel, T. (2014). *Human settlements, infrastructure, and spatial planning*.

Solanky, V., Singh, S., & Katiyar, S. K. (2018). Land surface temperature estimation using remote sensing data. In Hydrologic Modeling: Select Proceedings of ICWEES-2016 (pp. 343-351). Springer Singapore.

Souza Jr, C. M., Z. Shimbo, J., Rosa, M. R., Parente, L. L., A. Alencar, A., Rudorff, B. F., Hasenack, H., Matsumoto, M., G. Ferreira, L., Souza-Filho, P.W. & Azevedo, T. (2020). Reconstructing three decades of land use and land cover changes in brazilian biomes with landsat archive and earth engine. *Remote Sensing*, *12*(17), 2735.

Yang, Y., Cao, C., Pan, X., Li, X., & Zhu, X. (2017). Downscaling land surface temperature in an arid area by using multiple remote sensing indices with random forest regression. *Remote Sensing*, *9*(8), 789.